Hollow Mesoporous Organosilica Nanoparticles: A Generic Intelligent Framework-Hybridization Approach for Biomedicine

Yu Chen,[†,‡,#] Qingshuo Meng,[§,#] Meiying Wu,[†] Shige Wang,[†] Pengfei Xu,[§] Hangrong Chen,[†] Yaping Li,*[,§] Lingxia Zhang,[†] Lianzhou Wang,*[,‡] and Jianlin Shi*[,†]

[†]State Key Laboratory of High Performance Ceramics and Superfine Microstructure, Shanghai Institute of Ceramics, Chinese Academy of Sciences, Shanghai, 200050, P. R. China

[‡]Nanomaterials Center, School of Chemical Engineering and Australia Institute for Bioengineering and Nanotechnology, University of Queensland, Brisbane, Queensland 4072, Australia

[§]Shanghai Institute of Materia Medica, Chinese Academy of Sciences, Shanghai, 201203, P. R. China

Ⓢ *Supporting Information*

ABSTRACT: Chemical construction of molecularly organic–inorganic hybrid hollow mesoporous organosilica nanoparticles (HMONs) with silsesquioxane framework is expected to substantially improve their therapeutic performance and enhance the biological effects beneficial for biomedicine. In this work, we report on a simple, controllable, and versatile chemical homology principle to synthesize multiple-hybridized HMONs with varied functional organic groups homogeneously incorporated into the framework (up to quintuple hybridizations). As a paradigm, the hybridization of physiologically active thioether groups with triple distinctive disulfide bonds can endow HMONs with unique intrinsic reducing/acidic- and external high intensity focused ultrasound (HIFU)-responsive drug-releasing performances, improved biological effects (e.g., lowered hemolytic effect and improved histocompatibility), and enhanced ultrasonography behavior. The doxorubicin-loaded HMONs with concurrent thioether and phenylene hybridization exhibit drastically enhanced therapeutic efficiency against cancer growth and metastasis, as demonstrated both *in vitro* and *in vivo*.
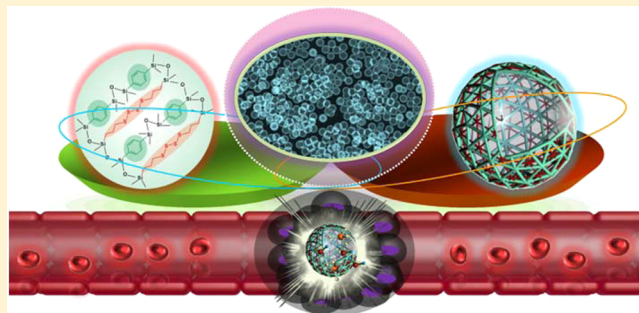
1. INTRODUCTION

Mesoporous silica nanoparticles (MSNs) are regarded as one of the most promising inorganic carriers in drug delivery systems (DDSs) for chemotherapy, which have been extensively explored in biomedicine for more than 13 years.[1,2] Although the high performances of MSNs have been demonstrated in drug/gene delivery,[3−13] diagnostic imaging,[14,15] photodynamic/photothermal therapy,[16−18] and even tissue engineering,[19,20] their clinical translations seem to have encountered great difficulties in the aspect of biosafety issue. Systematic *in vivo* biosafety evaluations have been carried out, including biodistribution, biodegradation, excretion, histocompatibility, hemocompatibility, etc.[21,22] The preliminary results seem promising, but the inert inorganic −Si−O−Si− framework of MSNs is their intrinsic drawback that is still under the big debate for further clinical translations.[1,22−24] Of particular promise is that the incorporation of physiologically active organic groups into the framework of MSNs can fast promote the clinical translations because these hybrid nanosystems can combine the features of both organic and inorganic nanosystems but overcome their drawbacks accordingly.[25−27]

Although organic modifications of the inner mesopores or outer particles' surfaces can bring specific functions, such as

targeting,[28] improved stability,[29] on-demand drug releasing,[6] and long circulation time,[30] such localized modifications will not change the intrinsic nature of −Si−O−Si− framework of MSNs. Alternatively, homogeneous incorporation/hybridization of functional organic groups into the framework of MSNs can produce molecularly organic–inorganic hybrid mesoporous organosilica nanoparticles (MONs) with silsesquioxane framework, which can significantly change the intrinsic framework nature of MSNs suitable for biomedical applications.[25−27,31] For instance, it has been demonstrated that the phenylene-bridged MSNs show enhanced therapeutic efficiency of focused ultrasound,[32] and the ethylene-bis(propyl)disulfide-based mesoporous organosilica exhibited the unique biodegradable behavior and pH-responsive drug-releasing performance.[33]

As a specific member of MSNs-based nanofamily, hollow MSNs (HMSNs) have attracted much greater attention due to their unique nanoscale hollow architectures, which can act as large reservoirs for guest molecule loading and reduce the deposition of foreign materials into bodies subsequently.[34,35] HMSNs with a pure −Si−O−Si− framework have been

synthesized via various soft-/hard-templating methods,[32] which can be defined as the first-generation HMSNs (Figure 1a).
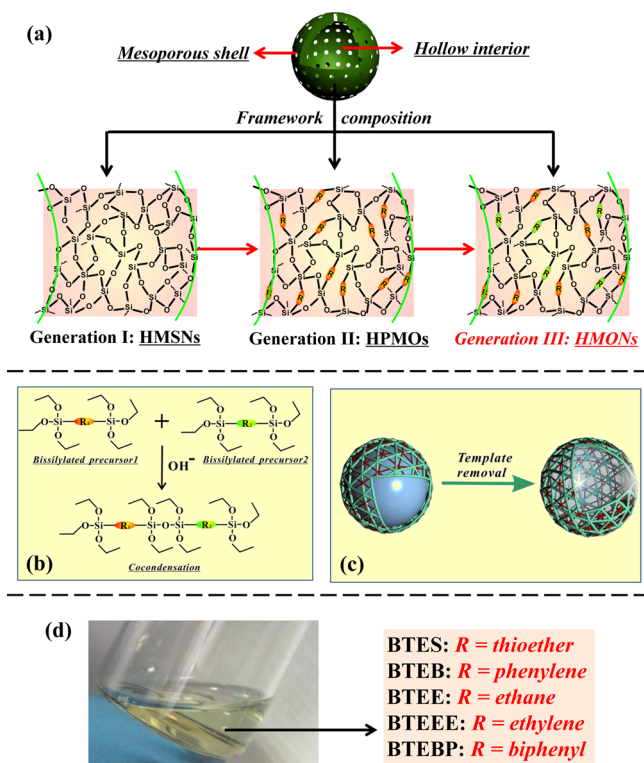

Figure 1. (a) Schematic illustration of the evolution of three generations of silica-based hollow mesoporous capsules classified in terms of chemical composition of the shell. (b) The chemical homology principle for constructing the hybrid silsesquioxane framework of HMONs. (c) The scheme of templating method to fabricate dual-functionalized HMONs (R_1: thioether, R_2: phenylene). (d) Photographic image of homogeneous solution of up to five bissilylated organosilica precursors miscible with each other, including BTES (R_1), BTEB (R_2), BTEEE (R_3), BTEE (R_4), and BTEBP (R_5).

Their morphology, particulate size, and pore diameter can also be precisely controlled simply by optimizing the core templates or other synthetic parameters based on typical sol−gel chemistry.[36] The fabrication of hollow periodic mesoporous organosilicas (HPMOs) with specific framework-incorporated biologically inert organic R moieties (R = phenyl (aromatic), ethyl (aliphatic), or vinyl (alkene) group) can be considered as the second generation of MSN-based hollow capsules.[26,37] Moreover, the incorporation of multiple R moieties with versatile specific functionalities, such as biologically active R moieties, remains a challenging topic, whereas it is expected to be capable of further improving their biological effect/biosafety and enhancing the therapeutic efficiency beneficial to biomedical applications. We define these multiple-hybridized hollow MONs (designated as HMONs) as the new third-generation MSNs-based hollow capsules, which, however, is not available in literature to date. In this article, we first propose a chemical homology mechanism to synthesize the third-generation HMONs with multiple molecularly organic−inorganic hybridizations (up to quintuple hybridizations). Subsequently, the composition−performance relationships of HMONs in biomedicine have been systematically clarified, both *in vitro* and *in vivo*. As a paradigm, we show that the molecular hybridization of physiologically active thioether group with

triple distinctive disulfide bonds can respond to both reducing microenvironment and focused ultrasound for dual stimuli-responsive drug releasing.

Figure 1b represents the chemical homology principle that the hydrolysis of bissilylated precursors is based on the formation of Si−OH at the end of bissilylated molecules under the assistance of an alkaline catalyst. The following condensation can generate −Si−O−Si− bonds to link different kinds of hydrolyzed bissilylated compounds, irrespective of the bridged organic R moieties within bissilylated precursors. Based on this mechanism, we can synthesize HMONs with multiple-incorporated R groups within the framework by a typical SiO_2-templating approach combined with silica-etching chemistry (Figure 1c). It is important to note that the different bissilylated precursors are usually miscible with each other (Figure 1d),[38] at least including bis[3-(triethoxysilyl)propyl]tetrasulfide (BTES, R_1 = thioether), bis(triethoxysilyl)phenylene (BTEB, R_2 = phenylene), bis(triethoxysilyl)ethylene (BTEEE, R_3 = ethylene), bis(triethoxysilyl)ethane (BTEE, R_4 = ethane), and bis(triethoxysilyl)biphenyl (BTEBP, R_5 = biphenyl), as investigated in this work. Such a chemical homology mechanism and high mutual miscible behavior of bissilylated precursors guarantee the further concurrent incorporations of versatile organic functional R groups into the framework of HMONs.

2. EXPERIMENTAL SECTION

2.1. Materials. Bis[3-(triethoxysilyl)propyl]tetrasulfide (BTES, R_1 = thioether) was obtained from Aladdin Industrial Inc. Bis(triethoxysilyl)ethylene (BTEEE, R_3 = ethylene) was bought from Gelest. Bis(triethoxysilyl)phenylene (BTEB, R_2 = phenylene), bis(triethoxysilyl)ethane (BTEE, R_4 = ethane), bis(triethoxysilyl)-biphenyl (BTEBP, R_5 = biphenyl), glutathione (GSH), and cetyltrimethylammonium bromide (C_{16}TAB) were purchased from Sigma-Aldrich. Tetraethyl orthosilicate (TEOS), ethanol, hydrofluoric acid (HF, 40%), and ammonia solution (25−28%) were obtained from Sinopharm Chemical Reagent Co. Phosphate buffer solution (PBS) was purchased from Shanghai Ruicheng Bio-Tech Co., Ltd. Chemotherapeutic agent doxorubicin (Dox) was obtained from Beijing HuaFeng United Technology Co., Ltd. All chemicals were used without further purification. Deionized water was used in all synthetic experiments.

2.2. Chemical Synthesis of Dual-Hybridized HMONs (R_1: thioether, R_2: phenylene). Organic R_1 and R_2 groups were concurrently incorporated into the framework of HMONs by employing the mixture of BTES and BTEB as the co-precursors. Monodispersed SiO_2 nanoparticles were initially synthesized as the hard template according to the typical Stöber method. Ethanol (74 mL), deionized water (10 mL), and ammonia solution (3.14 mL) were premixed, followed by quickly adding TEOS (6 mL). The silica colloidal solution was prepared by a further 1 h reaction at 30 °C in a water bath, which was then added into a mixture containing deionized water (100 mL) and C_{16}TAB solution (30 mL, V_{water}:V_{EtOH} = 2:1) dropwise. After further magnetic stirring for 30 min at 30 °C, another ammonia solution (3 mL) was added, followed by adding mixed organosilica precursors with different volume ratios (A: 0.8 mL BTEB and 0.2 mL BTES; B: 0.5 mL BTEB and 0.5 mL of BTES; C: 0.2 mL BTEB and 0.8 mL BTES). The coating reaction lasted for another 6 h, followed by centrifugation to collect the core/shell structured SiO_2@MONs. For etching process, half of the product of as-prepared SiO_2@MONs was dispersed into water by mild ultrasound treatment. HF (500 and 800 μL, respectively) was added into SiO_2@MONs dispersions at 60 °C for another 1 h of etching. The as-synthesized HMONs were collected by centrifugation and washed three times with deionized water. The surfactants (C_{16}TAB) were removed by the typical extraction approach in diluted HCl ethanol solution for 12 h at 80 °C (repeated three times). The final HMONs were then obtained

by centrifugation, washed with ethanol and water several times, and freeze dried under vacuum.

2.3. Synthesis of Triple-, Quadruple-, and Quintuple-Hybridized HMONs. The synthetic procedure for triple-, quadruple-, and quintuple-hybridized HMONs was similar to the process for dual-hybridized HMONs except for the substitution of organosilica precursors with corresponding multiple-precursor mixtures. The volumes of HF etchant used were 500 and 800 μL, respectively.

For triple-hybridized HMONs, the adopted volumes of BTEB, BTES, and BTEEE are described as follows: A: 0.5 mL BTEB, 0.5 mL BTES, 0.2 mL BTEEE; B: 0.5 mL BTEB, 0.5 mL BTES, 0.5 mL BTEEE; C: 0.5 mL BTEB, 0.5 mL BTES, 0.8 mL BTEEE.

For quadruple-hybridized HMONs, the added amounts of BTEB, BTES, BTEEE, and BTEE in the recipes are A: 0.3 mL BTEB, 0.3 mL BTES, 0.3 mL BTEEE, 0.3 mL BTEE; B: 0.3 mL BTEB, 0.3 mL BTES, 0.3 mL BTEEE, 0.5 mL BTEE.

For quintuple-hybridized HMONs, the employed volumes of BTEB, BTES, BTEEE, BTEE, and BTEBP are 0.3 mL BTEB, 0.3 mL BTES, 0.3 mL BTEEE, 0.3 mL BTEE, and 0.3 mL BTEBP.

2.4. Reducing Responsive Drug Releasing. Dox was encapsulated into HMONs by immersing dual-hybridized HMONs (20 mg) into Dox PBS solution (0.4 mg/mL, 20 mL). The mixture was stirred at room temperature in the dark for 24 h, followed by centrifugation to collect Dox-loaded HMONs. The supernatant was obtained for UV−vis characterization to determine the Dox-loading amount within HMONs.[26]

Reducing-responsive Dox releasing was conducted in PBS at the GSH concentrations of 5 and 10 mM. Typically, Dox-HMONs (3 mg) were sealed into a dialysis bag with a cutoff molecular weight of 5000 Da. The sealed dialysis bag was immersed into GSH solution (30 mL) at different concentrations (0, 5, and 10 mM), which was further put into a shaking table at the shaking speed of 100 rpm at 37 °C. The releasing medium was tested by UV−vis at given time to determine the released amount of Dox molecules.

2.5. HIFU-Triggered On-Demand Drug Releasing. The external high intensity focused ultrasound (HIFU) irradiation can trigger the Dox-releasing from HMONs. Typically, Dox-loaded HMONs powder (5 mg) was dispersed into PBS solution (1 mL) via a mild and short ultrasound treatment to improve the dispersity degree of nanoparticles. Then, the PBS solution containing Dox-HMONs was transferred into the dialysis bag with the cutoff molecular weight of 5000 Da, which was then put into another PBS with the volume of 50 mL. The dialysis bag containing Dox-HMONs was directly moved to the focal point of HIFU. The HIFU with pulse-wave mode was employed to act on Dox-HMONs. After HIFU irradiation, the releasing medium was tested by UV−vis to determine the Dox-releasing percentage. The power densities of HIFU irradiation were 100 and 200 W/cm², and the irradiation interval was 60 s. The adopted HIFU frequency was 1.0 MHz.

2.6. Cell Culture and Animals. *Cell Culture.* Dox-resistant breast cancer cell line (MCF-7/ADR) was cultured in RPMI 1640 containing 10% fetal bovine serum (FBS), 100 U/mL penicillin G sodium, 100 μg/mL streptomycin sulfate, and 1 μg/mL Dox. The 1 μg/mL Dox was added to stimulate the Dox resistance of MCF-7/ADR cells. Cells were cultured in a humidified and 5% CO₂ incubator at 37 °C.

Animals. Six week old female BALB/c nude mice (18−20 g) were purchased from Shanghai Experimental Animal Center (Shanghai). The *in vivo* experiments were performed under the guideline approved by the Institutional Animal Care and Use Committee of the Shanghai Institute of Materia Medica, Chinese Academy of Sciences.

2.7. *In Vivo* Chemotherapeutic Efficiency of Dox-HMONs To Inhibit the Tumor Growth and Metastasis. Female BALB/c nude mice with tumors on the right mammary gland were generated by injection of 1×10^5 4T1 cells. The tumors were allowed to grow to a volume of 100−200 mm³ before experiment. The tumor-bearing mice were randomly divided into four groups: group I receiving saline solution; group II receiving HMONs saline solution; group III receiving free Dox saline solution; and group IV receiving Dox-HMONs saline solution. Each group includes five mice ($n = 5$). The administration mode was intravenous injection. The equivalent Dox

dose was 2.5 mg/kg. Such an intravenous administration was repeated after 1 week of treatment. The tumor volume was monitored every 3 days. The tumor volume was calculated based on the following formula: $V = (W^2 \times L)/2$ (L: the longest size of tumor, W: the shortest diameter of perpendicular to length). When the chemotherapy was ended, the mice were sacrificed, and the tumors were taken out for photographing and testing of their weights. The tumors and lungs were photographed, and the metastatic nodules on the surface of lung were counted at the same time. Histopathological examination of tumor and lung was conducted by the typical hematoxylin and eosin (H&E) staining. The sections of tumors were co-incubated with anti-CD31 rabbit antibody, followed by counter-staining with hematoxylin, which was further observed in an optical microscope.

2.8. Characterizations. The microstructure of HMONs was characterized by transmission electron microscopy (TEM), which was recorded on a JEM-2100F electron microscope operated at 200 kV. Scanning electron microscopy (SEM) images were used to observe the morphology of HMONs on a field-emission Magellan 400 microscope (FEI Co.). N₂ adsorption−desorption isotherm and corresponding pore size distribution were acquired to characterize the mesoporous structure of HMONs on a Micrometitics Tristar 3000 system. Dynamic light scattering was tested to determine the particle sizes of HMONs on a Zetasizer Nanoseries (Nano ZS90). UV−vis spectra were recorded on a UV-3101PC Shimadzu spectroscope. Raman spectrum was acquired on a Thermofisher spectrometer (DXR) with the excitation wavelength of 633 nm. Confocal laser scanning microscopy (CLSM) images were obtained on FV1000, Olympus Co.

3. RESULTS AND DISCUSSION

It has been well-demonstrated that the disulfide bond is physiologically active, which can be broken up upon exposure to the reducing environment.[39,40] The hybridization of disulfide bond into silica framework is expected to endow the framework with physiologically responsive behavior. To validate this idea, BTES with organic thioether group (R_1 = thioether: $-Si-(CH_2)_3S-S-S(CH_2)_3Si-$) was co-hydrolyzed and co-condensed with BTEB (R_2 = phenylene: $-Si-C_6H_4-Si-$) to fabricate a unique dual-hybridized HMONs. Monodispersed SiO₂ nanoparticles were employed as the hard template to guarantee the high dispersity of following synthesized HMONs, which were further coated with a mesoporous organosilica layer by co-hydrolysis/condensation of BTES and BTEB at varied volume ratios ($V_{BTES}:V_{BTEB}$ = 1:4, 1:1, and 4:1). HMONs can be obtained by further etching away of the SiO₂ core in diluted HF solution based on a 'structural difference-based selective etching' strategy.[38] TEM images (Figure 2a,b) exhibit the high dispersity and apparent hollow structure of achieved HMONs (initial $V_{BTES}:V_{BTEB}$ = 1:1), as can be well-distinguished from the large contrasts between the core and the shell. Their high uniformity and well-defined spherical morphology are shown in SEM image (Figure 2c). Element mapping of HMONs (Figure 2d−h) not only gives the direct evidence of hollow nanostructure but also shows the homogeneous distribution of sulfur (Figure 2g) and carbon (Figure 2d) elements within the shell of HMONs.

HMONs with R_1 and R_2 hybridizations exhibit high hydrophilicity and dispersity in aqueous solution with an average hydrolyzed particle size of 402 nm (Figures S1 and S2). The ζ potential of HMONs under neutral condition (pH = 7.4) is −31.3 mV, which gives the significant decrease in acidic environment (Figure S3). Additionally, HMONs possess well-defined mesoporous structures (Figure S4) with a large surface area of 1005 m²/g, pore size of 3.8 nm, and high pore volume of 1.09 cm³/g. The compositional information on HMONs was
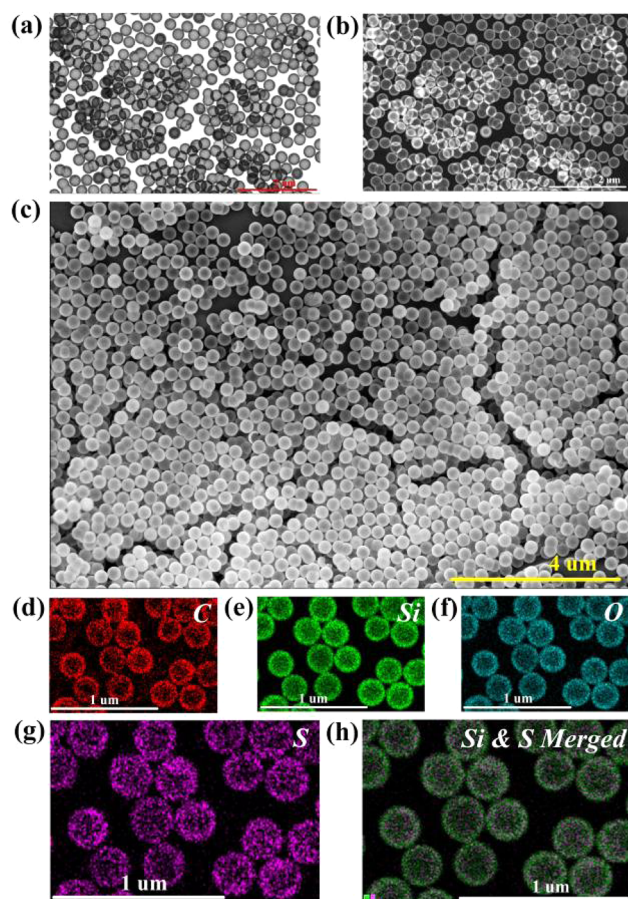
Figure 2. (a) Bright-field TEM, (b) dark-field TEM, and (c) SEM images of dual-hybridized HMONs (R$_1$: thioether, R$_2$: phenylene). (d–h) Element mapping of HMONs: (d) C, (e) Si, (f) O, (g) S, and (h) merged image of e and g.

further characterized by ^{29}Si magic-angle spinning (MAS) and ^{13}C cross-polarization MAS (CPMAS) solid-state NMR spectra (Figure 3). The ^{29}Si NMR spectrum (Figure 3a) shows the strong signals of T sites in the range of −50 to −90 ppm. The signals at −56.9, −69.3, and −79.7 ppm can be assigned to silicon resonances of T^1, T^2, and T^3 units [T^n = RSi-
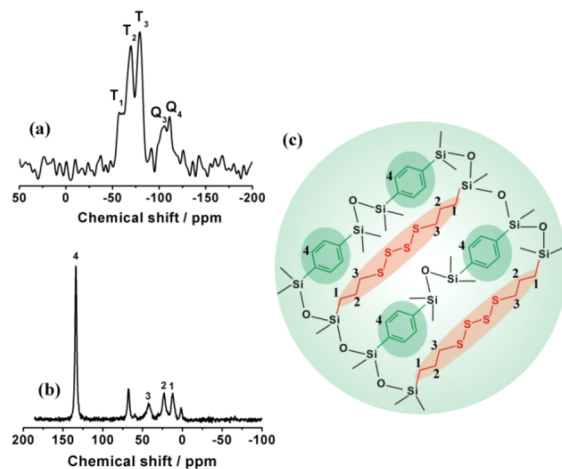

Figure 3. Solid-state (a) ^{29}Si and (b) ^{13}C CP/MAS NMR spectra of dual-hybridized HMONs. (c) Schematic illustration of dual-hybridized HMONs containing thioether (R$_1$) and phenylene (R$_2$) groups.

(OH)$_{3−n}$(OSi)$_n$, n = 1, 2, and 3], further demonstrating the formation of silsesquioxane hybrid composition.[41] The resonances in ^{13}C CPMAS NMR spectrum (Figure 3b) at 12.3, 23.8, 41.9, and 134.1 can be indexed to ^{1}C, ^{2}C, ^{3}C, and ^{4}C carbon species of −Si−^{1}CH$_2$−^{2}CH$_2$−^{3}CH$_2$−S−S−S−S−^{3}CH$_2$−^{2}CH$_2$−^{1}CH$_2$−Si− and −Si−^{4}C$_6$H$_4$−Si−, respectively,[41,42] indicating the presence of thioether (R$_1$) and phenylene (R$_2$) groups within the framework. The presence of −S−S− bonds was further demonstrated by Raman spectrum, which shows the specific stretching vibrations of −S−S− bond at the Raman shifts of 438 and 488 cm^{-1} (Figure 4). The stretching vibration of −S−C− at 636 cm^{-1} was also
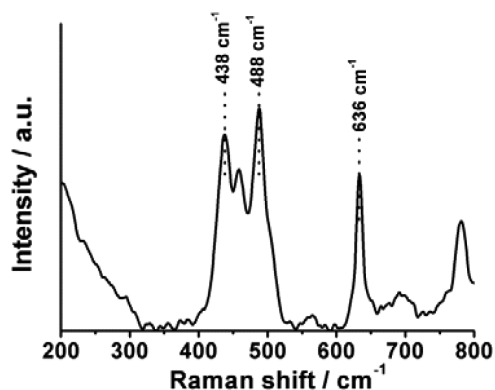

Figure 4. Raman spectra of dual-hybridized HMONs (R$_1$: thioether, R$_2$: phenylene).

observed.[42] Due to the simplicity of the synthetic procedure, several crucial compositional/structural parameters can be delicately optimized, such as the amounts of −S−S− bonds (Figure S5) and mesopore sizes (Figure S6).

Due to the versatile nature of chemical homology mechanism (Figure 1b), this synthetic protocol can be easily extended to fabricate HMONs with more types of incorporated functional organic R groups. The only necessary change during the synthesis is the introduction of more kinds of bissilylated organosilica precursors based on their high mutually miscible character (Figure 1d). Triple- (R$_1$ = thioether, R$_2$ = phenylene, and R$_3$ = ethylene; Figures S7–S10), quadruple- (R$_1$ = thioether, R$_2$ = phenylene, R$_3$ = ethylene, and R$_4$ = ethane; Figures S11−S14), and even quintuple-hybridized (R$_1$ = thioether, R$_2$ = phenylene, R$_3$ = ethylene, R$_4$ = ethane, and R$_5$ = biphenyl; Figures 5 and S15) HMONs can be successfully fabricated via the same mechanism and similar procedure. TEM images of quintuple-hybridized HMONs also exhibit the spherical morphology and hollow nanostructure (Figure 5a,d). High-magnification SEM (Figure 5e) image clearly shows the presence of well-defined mesopores in the shell of HMONs. The uniform distribution of C and S elements within the shell of HMONs was further demonstrated by the EDS element mapping (Figure 5f−j), which is further evidence of the molecular organic−inorganic hybridization of HMONs. Similar to the ^{29}Si NMR spectra of dual-, triple-, and quadruple-hybridized HMONs, the ^{29}Si NMR spectrum of quintuple-hybridized HMONs (Figure 6a) also shows the distinguishing signals of T sites, which can also be assigned to silicon resonances of T^1, T^2, and T^3 units [T^n = RSi(OH)$_{3−n}$(OSi)$_n$, n = 1, 2, and 3]. The specific resonances of ^{13}C NMR spectrum (Figure 6b) at 12.3, 23.8, 41.9, 134.1, 146.9, 4.4, and newly emerged 126.3 ppm can be indexed to ^{1}C, ^{2}C, ^{3}C, ^{4}C, ^{5}C, ^{6}C,
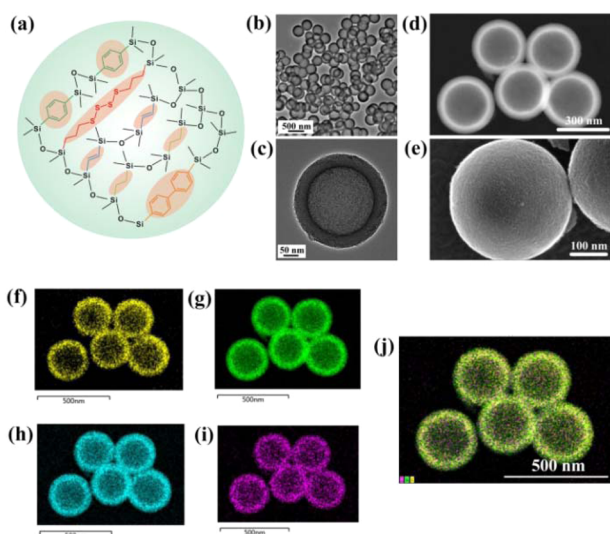
Figure 5. (a) Schematic illustration of quintuple-hybridized HMONs (R_1 = thioether, R_2 = phenylene, R_3 = ethylene, R_4 = ethane, and R_5 = biphenyl). (b, c) Bright-field TEM and (d) dark-field TEM images of quintuple-hybridized HMONs. (e) High-magnification SEM image of HMONs. (f–j) EDS elemental mapping images of (f) C, (g) Si, (h) O, (i) S, and (j) merged image of f, g, and i of quintuple-hybridized HMONs.
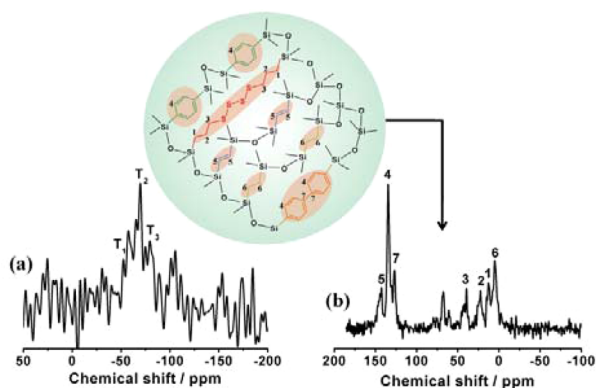

Figure 6. Solid-state (a) ^{29}Si and (b) ^{13}C CP/MAS NMR spectra of quintuple-hybridized HMONs (R_1 = thioether, R_2 = phenylene, R_3 = ethylene, R_4 = ethane, and R_5 = biphenyl).

and ^{7}C carbon species of $-Si-^1CH_2-^2CH_2-^3CH_2-S-S-S-S-^3CH_2-^2CH_2-^1CH_2-Si-$, $-Si-^4C_6H_4-Si-$, $-Si-^5C\equiv^5C-Si-$, $-Si-^6C-^6C-Si-$, and $-Si-C_6H_4-^7C_6H_4-Si-$. These ^{29}Si and ^{13}C NMR spectra further strongly demonstrate that five organic R (R_1 = thioether, R_2 = phenylene, R_3 = ethylene, R_4 = ethane, and R_5 = biphenyl) groups have been successfully hybridized into the framework of HMONs. Importantly, the multiple-hybridized HMONs still maintain the well-defined mesoporous structures (Figure S16 and Table S1). Such a molecularly organic–inorganic hybridization methodology provides a versatile protocol to fabricate new HMON-based material families to satisfy various application requirements.

We have previously demonstrated that the incorporation of inert organic phenylene (R_2) group into the $-Si-O-Si-$ framework can substantially decrease the hemolytic effect against red blood cells due to the large decrease of surface-exposed silanol (Si–OH).[26] Similarly, the co-incorporation of thioether (R_1) and phenylene (R_2) groups can also endow HMONs with lowered hemolytic effect, which, however, is

slightly higher than that by single phenylene hybridization (Figure S17). HMONs with dual hybridization still possess high *in vivo* histocompatibility (Figure S18). In addition, HMONs exhibit the time-dependent biodegradation behavior in simulated body fluid at the GSH concentration of 10 mM (Figure S19). Interestingly, the incorporation of thioether groups with relatively long molecular chain can substantially improve the ultrasound imaging performance of HMONs compared to phenylene-hybridized HPMOs (Figures S20 and S21). The high ultrasonography behavior of dual-hybridized HMONs is rationalized by the change of the overall shell stiffness based on the fact that the long-chain thioether group will render HMONs' shell enhanced elasticity to respond to the ultrasound irradiation.[43]

The incorporation of phenylene (R_2) and thioether (R_1) groups within the framework of HMONs facilitates the encapsulation of aromatic guest molecules in the HMONs via both $\pi-\pi$ supramolecular stacking and hydrophobic–hydrophobic interaction. The drug-loading capacity of HMONs toward anticancer drug Dox reached 148 mg/g. Disulfide bond ($-S-S-$) has been well demonstrated to be broken by the intracellular GSH via the redox reaction.[40] Thus, it is anticipated that the triple disulfide bonds in a thioether group within the framework are highly responsive to reducing environments to quickly trigger the releasing of loaded guest molecules (Figure 7a). To validate this assumption, the releasing patterns of Dox-loaded HMONs were monitored at different GSH concentrations (0, 5, and 10 mM) in PBS. GSH concentrations of 5 and 10 mM were adopted because the intracellular GSH concentrations are in the range of 1−10 mM, while the tumor cells exhibit significantly higher GSH concentrations.[40] The release of Dox in pure PBS shows a slow and sustained profile with only 21.8% releasing percentage in 24 h (Figure 7b). Upon the addition of GSH, the 24 h releasing amount is substantially increased to 47.2% and 69.0% at the GSH concentrations of 5 and 10 mM, respectively. After the reduction and subsequent cleavage of disulfide bonds within the thioether group, the initially established $\pi-\pi$ supramolecular stacking and hydrophobic–hydrophobic interaction between the framework and the aromatic Dox molecules can be broken up, leading to the substantially increased drug-releasing rates.

It has been demonstrated that the effect of ultrasonic cavitation can cause the solvodynamic shear to induce the scission of polymer chain.[44] In addition, the disulfide bond can be easily cleaved by focused ultrasound due to their relatively low dissociation energy (∼268 kJ/mol) and long bond length (0.203 nm) compared to C–C bond (dissociation energy: 347 kJ/mol; bond length: 0.154 nm).[44,45] In addition, the weak noncovalent $\pi-\pi$ supramolecular stacking and hydrophobic–hydrophobic interaction between the aromatic drug molecules and HMONs' framework can also be disrupted by the mechanical/cavitation effects during exposure to the focused ultrasound. As shown in Figure 7c, the releasing rate of Dox is extremely low at the initial stage, but upon exposure to HIFU, a unique pulsatile Dox-releasing pattern can be obtained by switching the ON/OFF status of HIFU. Within a short duration of about 100 min, the Dox-releasing percentage can reach as high as 49% and 87% after exposure to HIFU at the power densities of 100 and 200 W/cm², respectively. In addition, the Dox-loaded HMONs also exhibit the pH-dependent releasing profiles where the acidic environment can fast trigger the releasing of Dox from HMONs (Figure
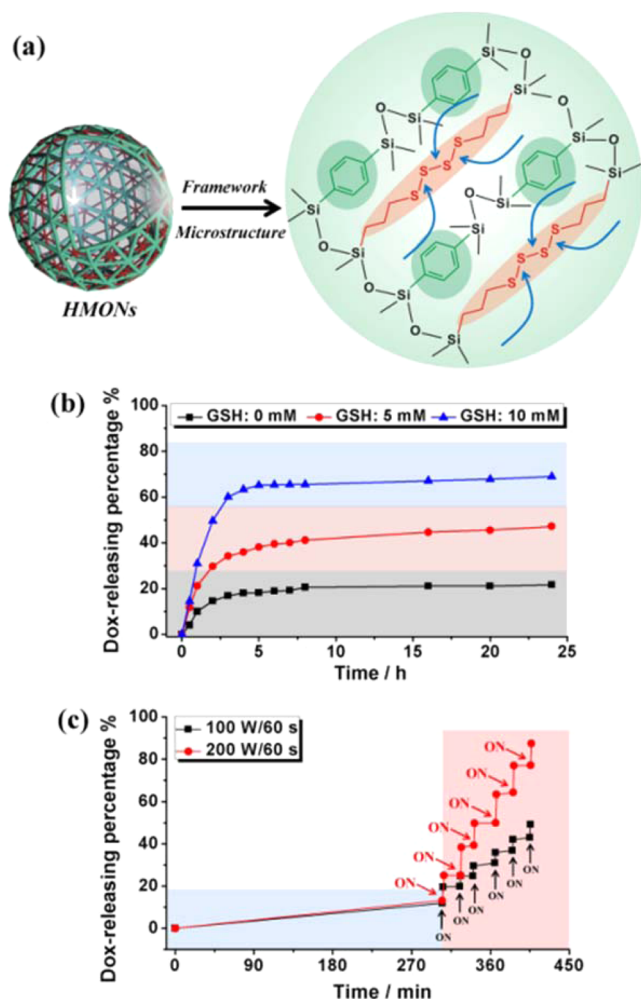
Figure 7. (a) Schematic illustration of the framework composition of dual-hybridized HMONs (R_1: thioether, R_2: phenylene). (b) Cumulative Dox-releasing percentages at the GSH concentrations of 0, 5, and 10 mM in PBS solutions. (c) HIFU-triggered Dox-releasing profiles at different power densities (100 and 200 W/cm^2, 60 s irradiation).

S22). The triple responsiveness of HMONs for Dox-releasing builds a unique drug–framework interaction-based intelligent nanosystem that responds to either intrinsic microenvironment of cancer cells (e.g., reducing/acidic condition) or artificially introduced external remote triggers (e.g., focused ultrasound).

HMONs display low cytotoxicities against MCF-7/ADR cancer cells even at the high concentration of 600 μg/mL (Figure S23). The *in vitro* HMONs-mediated intracellular delivery of Dox can enhance the Dox concentrations within Dox-resistant MCF-7/ADR cancer cells (Figure S24). CLSM (Figure S25) clearly shows the intracellular accumulation of Dox-loaded HMONs and subsequent intracellular Dox releasing. HMON-mediated Dox delivery can also accelerate the apoptosis and necrosis of MCF-7/ADR cancer cells, as demonstrated by the typical flow cytometry and fluorescence-activated cell-sorting protocols (Figure S26). Higher chemo-therapeutic efficiency was further demonstrated by the typical MTT assay (Figure S27). Thus, such an accelerated apoptosis/ necrosis of MCF-7/ADR cancer cells and correspondingly enhanced *in vitro* therapeutic outcome can be reasonably attributed to the enhanced accumulation of intracellular Dox concentration mediated by HMONs, reducing sensitive drug

releasing from the carrier and the consequently restored Dox sensitivity of the cancer cells.

The therapeutic efficiency of HMONs for *in vivo* anticancer drug delivery/chemotherapy was assessed on 4T1 orthotopic mammary tumor spontaneous metastasis xenograft. HMONs are able to accumulate within tumor tissues with relatively high amounts (Figure S28). The tumoricidal efficiency of Dox-loaded HMONs is significantly higher than free Dox (Figure 8a). The tumor volume (Figure 8b) and weight (Figure 8c) in
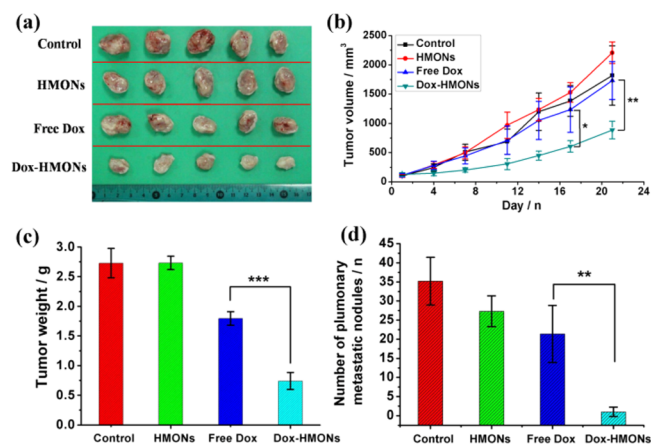

Figure 8. (a) Photographic images of tumors after different treatments. (b) The tumor volume changes as a function of time after different treatments ($n = 5$). (c) The tumor weights at the end of treatment. (d) The number of pulmonary metastatic nodules in lungs of mice after different treatments. **$P < 0.01$, ***$P < 0.001$.

the Dox-HMONs group were only 48.7% and 27.2% of that of the saline group, significantly lower than those of free Dox group (tumor volume: 95.2%, tumor weight: 65.7% of the saline group).

Importantly, the high tumor-suppression outcome results in the substantially inhibited tumor metastasis to lungs. The number of pulmonary metastatic nodules in lungs of Dox-HMONs group was as low as 2.8% of the saline group (Figure 8d), substantially lower than that of free Dox group (61% of the saline group).

Significantly enhanced tumor destruction and cell apoptosis of Dox-HMONs group can be observed by pathological hematoxylin and eosin stain (H&E) analysis (Figure 9a) and TUNEL staining (Figure 9b), indicating the high tumoricidal efficiency by Dox-HMONs. The metastasis of tumors into lungs was further demonstrated by counting the tumor metastasis nodules (Figure 9c) and the corresponding H&E pathological analysis (Figure 9d), which exhibits substantially reduced macrometastatic foci in the lungs of Dox-HMONs group. Importantly, the Dox delivery via HMONs highly favors the *in vivo* anti-angiogenesis effects as demonstrated by the immunohistochemical staining CD31 analysis (Figure 9e). Thus, the delivery of Dox mediated by HMONs can bring substantially enhanced destruction/apoptosis effects against tumors, significantly inhibited tumor metastasis and decreased angiogenesis.

Typically, inorganic SiO$_2$ nanoparticles and organic carriers possess their own intrinsic unique performances for bio-medicine. For instance, SiO$_2$ nanoparticles show high stability, tunable morphology/nanostructures, easy functionalizations, and relatively high biocompatibility. Comparatively, traditional organic carriers have the specific properties of high
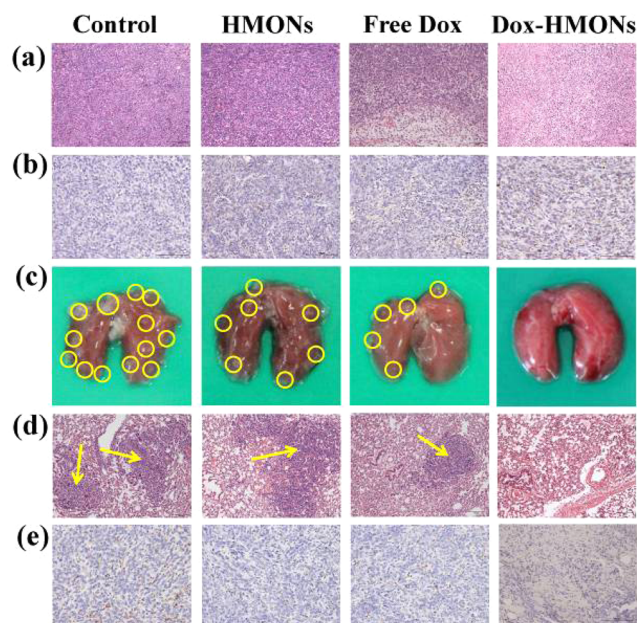
Figure 9. (a) H&E and (b) TUNEL staining images of tumor at the end of different treatments. (c) Photographic images of the lungs at the end of treatments and (d) corresponding histological analysis by H&E staining (arrows show the pulmonary metastasis). (e) Immunohistochemical staining analysis of tumors for CD31 after the treatment with saline, free Dox, and Dox-HMONs.

Figure 10. (a) Summary of the two typical organic−inorganic hybridization modes for biomedicine. (b) Schematic illustration of dual-hybridized HMONs for *in vivo* stimuli-responsive drug delivery.

biocompatibility, easy biodegradation, abundant organic functional groups, and relatively high tumor accumulations. Combining these two material systems together can endow the organic−inorganic hybrid nanosystems with the combined corresponding advantages of both inorganic SiO_2 nanoparticles and organic carriers.

There are two typical organic−inorganic hybridization approaches (Figure 10a). One is the surface modification using organic ligands and the other is framework hybridization. Typically, the organic modification on the surface of nanoparticles or mesopores by silane coupling agent can be used for some specific purposes such as targeting modifications, nanovalve installations for stimuli-responsive drug releasing, improving the stability of nanoparticles in physiological environment, etc. However, such a hybridization mode cannot change the compositional essence of SiO_2 because these organic groups are simply grafted onto the surface. Comparatively, the framework hybridizations by using bissilylated organosilica precursors change the intrinsic nature of SiO_2 framework because the introduced organic groups are homogeneously and molecularly incorporated into the Si−O−Si bonds. This hybridization mode can improve the biological effects and biosafety of organosilica nanoparticles and endow the nanocarriers with the specific functions by choosing appropriate bissilylated organosilica precursors with varied functional organic groups.

This work not only provides a generic synthetic method to incorporate diverse and even multiple functional organic groups into −Si−O−Si− bonds for framework organic hybridization but also provides the new paradigm that the incorporation of physiologically active organic groups can bring with specific functions. The introduced thioether containing triple disulfide bonds can respond to both the intrinsic reducing microenviron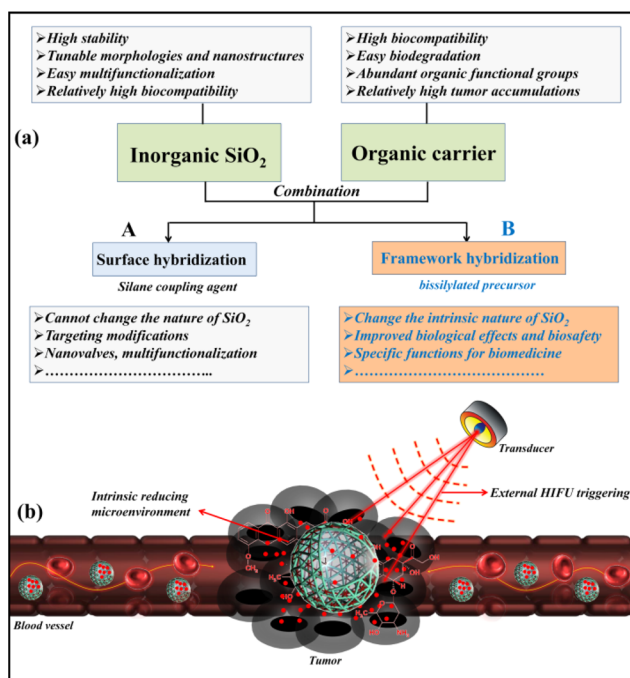ment of tumor tissues and external HIFU irradiations for stimuli-responsive intelligent drug releasing (Figure 10b). Such a construction methodology for triggered drug-releasing is significantly different from most reported installations of nanovalves onto the surface of mesopores, which typically require precisely controlled, time-consuming, and costly multiple modification steps to build various nanovalves. In comparison, this method is very simple. The introduction of thioether and phenylene groups can not only interact with drug molecules via either hydrophobic−hydrophobic interaction and/or $\pi-\pi$ supramolecular stacking to guarantee the slow releasing of drugs before they reach the tumor target but also release the loaded cargos by either the intrinsic or external triggers (Figure 10b). The surface groups (e.g., Si−OH) can be further used for some other specific purposes, such as targeting. Based on this consideration, the introduction of other functional groups with fast biodegradation behavior or contrast-enhanced imaging performance can either tune the biodegradation rates of organosilica nanoparticles or endow them with unique theranostic (concurrent diagnostic imaging and therapy) properties. Thus, this framework hybridization strategy based on the introduction of functional organic groups is expected to further promote the clinical translation of SiO_2-based nanosystems.

4. CONCLUSIONS

In summary, we have developed a simple, efficient, and versatile chemical homology principle to synthesize a new family of third-generation HMONs with multiple organic groups incorporated within the organosilica framework. Up to quintuple different types of functional R groups can be concurrently and homogeneously hybridized into HMONs. In particular, the incorporation of physiologically active thioether groups with disulfide bonds enables unique reducing and HIFU-responsive drug-releasing performance, specific biological effects, and enhanced ultrasonography behavior for

HMONs-based drug delivery systems. Importantly, the Dox-loaded HMONs exhibit remarkably enhanced antitumor therapeutic efficiency both *in vitro* and *in vivo*. Such a versatile molecularly organic–inorganic hybridization strategy for tuning the chemical composition of HMONs provides an alternative but effective route to endow them with specific functionalities and biological behaviors, which show the great clinical benefit and translation potential than traditional HMSNs. In addition to biomedical applications, these HMONs are expected to find wider applications in catalytic reaction, separation, energy storage, etc., which is strongly dependent on the practical requirements and types of incorporated organic R groups.

■ ASSOCIATED CONTENT

Ⓢ Supporting Information

Experimental section, additional characterization data of multiple-hybridized HMONs, and *in vitro* biological effects/therapeutic outcome. This material is available free of charge via the Internet at http://pubs.acs.org.

■ AUTHOR INFORMATION

Corresponding Authors
jlshi@mail.sic.ac.cn
l.wang@uq.edu.au
ypli@mail.shcnc.ac.cn

Author Contributions
#These authors contributed equally.

Notes
The authors declare no competing financial interest.

■ ACKNOWLEDGMENTS

■ REFERENCES

(1) Chen, Y.; Chen, H.; Shi, J. *Adv. Mater.* **2013**, *25*, 3144.
(2) Lee, J. E.; Lee, N.; Kim, T.; Kim, J.; Hyeon, T. *Acc. Chem. Res.* **2011**, *44*, 893.
(3) Ambrogio, M. W.; Thomas, C. R.; Zhao, Y. L.; Zink, J. I.; Stoddartt, J. F. *Acc. Chem. Res.* **2011**, *44*, 903.
(4) Xia, T. A.; Kovochich, M.; Liong, M.; Meng, H.; Kabehie, S.; George, S.; Zink, J. I.; Nel, A. E. *ACS Nano* **2009**, *3*, 3273.
(5) Tang, F. Q.; Li, L. L.; Chen, D. *Adv. Mater.* **2012**, *24*, 1504.
(6) Zhu, Y. F.; Shi, J. L.; Shen, W. H.; Dong, X. P.; Feng, J. W.; Ruan, M. L.; Li, Y. S. *Angew. Chem., Int. Ed.* **2005**, *44*, 5083.
(7) Slowing, I. I.; Vivero-Escoto, J. L.; Wu, C. W.; Lin, V. S. Y. *Adv. Drug Delivery Rev.* **2008**, *60*, 1278.
(8) Vallet-Regi, M.; Balas, F.; Arcos, D. *Angew. Chem., Int. Ed.* **2007**, *46*, 7548.
(9) Singh, N.; Karambelkar, A.; Gu, L.; Lin, K.; Miller, J. S.; Chen, C. S.; Sailor, M. J.; Bhatia, S. N. *J. Am. Chem. Soc.* **2011**, *133*, 19582.
(10) Yang, P. P.; Gai, S. L.; Lin, J. *Chem. Soc. Rev.* **2012**, *41*, 3679.
(11) Ashley, C. E.; Carnes, E. C.; Phillips, G. K.; Padilla, D.; Durfee, P. N.; Brown, P. A.; Hanna, T. N.; Liu, J. W.; Phillips, B.; Carter, M. B.; Carroll, N. J.; Jiang, X. M.; Dunphy, D. R.; Willman, C. L.; Petsev, D. N.; Evans, D. G.; Parikh, A. N.; Chackerian, B.; Wharton, W.; Peabody, D. S.; Brinker, C. J. *Nat. Mater.* **2011**, *10*, 389.
(12) Hou, Z.; Zhang, C.; Li, C.; Xu, Z.; Cheng, Z.; Li, G.; Wang, W.; Peng, C.; Lin, J. *Chem.—Eur. J.* **2010**, *16*, 14513.
(13) Gai, S. L.; Yang, P. P.; Li, C. X.; Wang, W. X.; Dai, Y. L.; Niu, N.; Lin, J. *Adv. Funct. Mater.* **2010**, *20*, 1166.
(14) Kim, J.; Kim, H. S.; Lee, N.; Kim, T.; Kim, H.; Yu, T.; Song, I. C.; Moon, W. K.; Hyeon, T. *Angew. Chem., Int. Ed.* **2008**, *47*, 8438.
(15) Lee, J. E.; Lee, N.; Kim, H.; Kim, J.; Choi, S. H.; Kim, J. H.; Kim, T.; Song, I. C.; Park, S. P.; Moon, W. K.; Hyeon, T. *J. Am. Chem. Soc.* **2010**, *132*, 552.
(16) Liu, H. Y.; Chen, D.; Li, L. L.; Liu, T. L.; Tan, L. F.; Wu, X. L.; Tang, F. Q. *Angew. Chem., Int. Ed.* **2011**, *50*, 891.
(17) Liu, H. Y.; Liu, T. L.; Wu, X. L.; Li, L. L.; Tan, L. F.; Chen, D.; Tang, F. Q. *Adv. Mater.* **2012**, *24*, 755.
(18) Gary-Bobo, M.; Mir, Y.; Rouxel, C.; Brevet, D.; Basile, I.; Maynadier, M.; Vaillant, O.; Mongin, O.; Blanchard-Desce, M.; Morere, A.; Garcia, M.; Durand, J.-O.; Raehm, L. *Angew. Chem., Int. Ed.* **2011**, *50*, 11425.
(19) Zhu, M.; Wang, H. X.; Liu, J. Y.; He, H. L.; Hua, X. G.; He, Q. J.; Zhang, L. X.; Ye, X. J.; Shi, J. L. *Biomaterials* **2011**, *32*, 1986.
(20) Vallet-Regi, M. *Chem.—Eur. J.* **2006**, *12*, 5934.
(21) Li, Z. X.; Barnes, J. C.; Bosoy, A.; Stoddart, J. F.; Zink, J. I. *Chem. Soc. Rev.* **2012**, *41*, 2590.
(22) Rosenholm, J. M.; Mamaeva, V.; Sahlgren, C.; Linden, M. *Nanomedicine* **2012**, *7*, 111.
(23) He, Q. J.; Zhang, Z. W.; Gao, F.; Li, Y. P.; Shi, J. L. *Small* **2011**, *7*, 271.
(24) Lin, Y. S.; Hurley, K. R.; Haynes, C. L. *J. Phys. Chem. Lett.* **2012**, *3*, 364.
(25) Urata, C.; Yamada, H.; Wakabayashi, R.; Aoyama, Y.; Hirosawa, S.; Arai, S.; Takeoka, S.; Yamauchi, Y.; Kuroda, K. *J. Am. Chem. Soc.* **2011**, *133*, 8102.
(26) Chen, Y.; Xu, P. F.; Chen, H. R.; Li, Y. S.; Bu, W. B.; Shu, Z.; Li, Y. P.; Zhang, J. M.; Zhang, L. X.; Pan, L. M.; Cui, X. Z.; Hua, Z. L.; Wang, J.; Zhang, L. L.; Shi, J. L. *Adv. Mater.* **2013**, *25*, 3100.
(27) Teng, Z.; Wang, S.; Su, X.; Chen, G.; Liu, Y.; Luo, Z.; Luo, W.; Tang, Y.; Ju, H.; Zhao, D.; Lu, G. *Adv. Mater.* **2014**, *26*, 3741.
(28) Pan, L. M.; He, Q. J.; Liu, J. N.; Chen, Y.; Ma, M.; Zhang, L. L.; Shi, J. L. *J. Am. Chem. Soc.* **2012**, *134*, 5722.
(29) Ma, K.; Sai, H.; Wiesner, U. *J. Am. Chem. Soc.* **2012**, *134*, 13180.
(30) Meng, H.; Xue, M.; Xia, T.; Ji, Z. X.; Tarn, D. Y.; Zink, J. I.; Nel, A. E. *ACS Nano* **2011**, *5*, 4131.
(31) Della Rocca, J.; Huxford, R. C.; Comstock-Duggan, E.; Lin, W. *Angew. Chem., Int. Ed.* **2011**, *50*, 10330.
(32) Qian, X.; Wang, W.; Kong, W.; Chen, Y. *RSC Adv.* **2014**, *4*, 17950.
(33) Croissant, J.; Cattoen, X.; Man, M. W. C.; Gallud, A.; Raehm, L.; Trens, P.; Maynadier, M.; Durand, J.-O. *Adv. Mater.* **2014**, *26*, 6174.
(34) Chen, Y.; Chen, H. R.; Guo, L. M.; He, Q. J.; Chen, F.; Zhou, J.; Feng, J. W.; Shi, J. L. *ACS Nano* **2010**, *4*, 529.
(35) Chen, Y.; Chen, H. R.; Sun, Y.; Zheng, Y. Y.; Zeng, D. P.; Li, F. Q.; Zhang, S. J.; Wang, X.; Zhang, K.; Ma, M.; He, Q. J.; Zhang, L. L.; Shi, J. L. *Angew. Chem., Int. Ed.* **2011**, *50*, 12505.
(36) Li, Y.; Shi, J. *Adv. Mater.* **2014**, *26*, 3176.
(37) Djojoputro, H.; Zhou, X. F.; Qiao, S. Z.; Wang, L. Z.; Yu, C. Z.; Lu, G. Q. *J. Am. Chem. Soc.* **2006**, *128*, 6320.
(38) Chen, Y.; Chen, H. R.; Shi, J. L. *Acc. Chem. Res.* **2014**, *47*, 125.
(39) Liu, R.; Zhao, X.; Wu, T.; Feng, P. Y. *J. Am. Chem. Soc.* **2008**, *130*, 14418.
(40) Lee, M. H.; Yang, Z.; Lim, C. W.; Lee, Y. H.; Dongbang, S.; Kang, C.; Kim, J. S. *Chem. Rev.* **2013**, *113*, 5071.
(41) Kim, J. H.; Fang, B.; Song, M. Y.; Yu, J.-S. *Chem. Mater.* **2012**, *24*, 2256.
(42) Liu, J.; Yang, Q.; Zhang, L.; Jiang, D.; Shi, X.; Yang, J.; Zhong, H.; Li, C. *Adv. Funct. Mater.* **2007**, *17*, 569.
(43) Lin, P. L.; Eckersley, R. J.; Hall, E. A. H. *Adv. Mater.* **2009**, *21*, 3949.

(44) Li, Y.; Tong, R.; Xia, H.; Zhang, H.; Xuan, J. *Chem. Commun.* **2010**, *46*, 7739.

(45) Wang, X.; Chen, H.; Zhang, K.; Ma, M.; Li, F.; Zeng, D.; Zheng, S.; Chen, Y.; Jiang, L.; Xu, H.; Shi, J. *Small* **2014**, *10*, 1403.

16334

dx.doi.org/10.1021/ja508721y | *J. Am. Chem. Soc.* 2014, 136, 16326−16334